Perovskite Solar Cells

Deutsche Ausgabe: DOI: 10.1002/ange.201606801
Internationale Ausgabe: DOI: 10.1002/anie.201606801

Ion-Exchange-Induced 2D–3D Conversion of $HMA_{1-x}FA_xPbI_3Cl$ Perovskite into a High-Quality $MA_{1-x}FA_xPbI_3$ Perovskite

*Ge Li, Taiyang Zhang, Nanjie Guo, Feng Xu, Xufang Qian, and Yixin Zhao**

Abstract: *High-quality phase-pure $MA_{1-x}FA_xPbI_3$ planar films (MA = methylammonium, FA = formamidinium) with extended absorption and enhanced thermal stability are difficult to deposit by regular simple solution chemistry approaches owing to crystallization competition between the easy-to-crystallize but unwanted δ-$FAPbI_3$/$MAPbI_3$ and $FA_xMA_{1-x}PbI_3$ requiring rigid crystallization conditions. Here A 2D–3D conversion to transform compact 2D mixed composition $HMA_{1-x}FA_xPbI_3Cl$ perovskite precursor films into 3D $MA_{1-x}FA_xPbI_3$ (x = 0.1–0.9) perovskites is presented. The designed Cl/I and H/FA(MA) ion exchange reaction induced fast transformation of compact 2D perovskite film, helping to form the phase-pure and high quality $MA_{1-x}FA_xPbI_3$ without δ-$FAPbI_3$ and $MAPbI_3$ impurity. In all, we successfully developed a facile one-step method to fabricate high quality phase-pure $MA_{1-x}FA_xPbI_3$ (x = 0.1–0.9) perovskite films by 2D–3D conversion of $HMA_{1-x}FA_xPbI_3Cl$ perovskite. This 2D–3D conversion is a promising strategy for lead halide perovskite fabrication.*

Lead halide perovskite solar cells have progressed up to about 22% certified efficiency in the past years.[1–15] The formamidinium (FA) based perovskites such as $FAPbI_3$ or MA-FA mixed $MA_{1-x}FA_xPbI_3$ (MA = methylammonium) have attracted more and more attention owing to their advantages of better thermal stability and extended absorption range compared to the well-studied $CH_3NH_3PbI_3$ ($MAPbI_3$) lead halide perovskites.[16–24] Although so many solution chemistry approaches with advantages of low cost and effectiveness have been developed for fabrication of high-efficiency $CH_3NH_3PbI_3$ ($MAPbI_3$) perovskite solar cells,[14,15,25–31] there is less solution chemistry deposition techniques for depositing high-quality phase-pure $MA_{1-x}FA_xPbI_3$ perovskite planar films. It is difficult to obtain phase-pure $MA_{1-x}FA_xPbI_3$ perovskite by solution chemistry because of the competition formation of easy-to-crystalize δ-$FAPbI_3$/$MAPbI_3$ and phase-pure $MA_{1-x}FA_xPbI_3$. This is due to the different steric effect of MA^+ and FA^+ cation with $[PbX_6]^{4-}$ units in the crystal lattice. Furthermore, the different steric effect of MA and FA cations make the excess MAI and FAI in two-step method compete to intercalate into perovskite crystal lattice, leading to uncertainty in the FA/MA ratios.[18] Consequently, it is difficult to prepare high-quality phase-pure $MA_{1-x}FA_xPbI_3$ without δ-$FAPbI_3$ impurity by the regular one-step or two-step methods. In the popular solvent engineering method, the $MA_{1-x}FA_xI$ and PbI_2 precursors also form the unwanted δ-$FAPbI_3$ mixed with $MAPbI_3$.[3] To solve this problem, the Br is usually adopted in solvent engineering to adjust the tolerant factor to help form phase-pure FA or FA-MA mixed perovskite, but the Br could broaden the band gaps to narrow the absorbance.[3,20] Recently, Han and co-workers have successfully developed a novel two-step method to prepare $MA_{1-x}FA_xPbI_3$ using $PbI_2{\cdot}x$FAI precursor films with fixed FAI stoichiometry for MAI intercalation.[23] In this novel stoichiometric controlled method, a rigid high temperature with narrow range is still critical to form the phase pure $PbI_2{\cdot}x$FAI precursor and $MA_{1-x}FA_xPbI_3$ perovskite. It is necessary to develop a general and facile solution method to prepare the phase-pure FA-MA mixed perovskite. The layer material precursor such as PbI_2 is an ideal candidate for preparation of compact perovskite films. In the two-step method, the layer structured PbI_2 is intercalated into 3D perovskite and the intercalation process involves lots of technique problems such as volume expansion because the size of $MAPbI_3$ is almost twice as PbI_2.[15,20,32]

In this 2D–3D intercalation process, the layer-structured 2D PbI_2 precursor is expanded into a 3D structure. Inspired by this concept of using a high quality precursor film, we developed a facile one-step strategy to transform the high-quality layer structure 2D mixed composite perovskite into 3D $MA_{1-x}FA_xPbI_3$ perovskite by an ion-exchange reaction. The layer-structured 2D organic/inorganic lead halide perovskites of A_2BX_4 (A = organic cation, B = Pb, X = I,Br,Cl) are a popular perovskite with various applications.[33–35] The conversion of 2D A_2BX_4 perovskite into 3D ABX_3 involving ion/cation exchange reaction would lead to release of the extra AX. To facilitate the ion/cation exchange reaction for the 2D/3D conversion, it is necessary to select some A and X candidate with weaker interaction in the crystal structure than the remaining A and X in the final ABX_3. Previous reports have suggested that the Cl has much weaker bond affinity to Pb than I and the MA(FA) trend to cation exchange with H in $HPbI_3$ frame.[22,25,36] To facilitate the ion-exchange reaction to induce the 2D perovskite conversion, the Cl with 1:3 molar ratio to I and the smallest cation H with 1:1 molar ratio to FA/MA mixture were adapted in our designed A_2BX_4 structure. As illustrated in Scheme 1, we developed a 2D perovskite precursor of mixed composition $HMA_{1-x}FA_xPbI_3Cl$, which can be facilely prepared by using stoichiometric $[HCl + (1-x)MAI + x\,FAI + PbI_2]$ mixture precursor solutions.

[*] G. Li, T. Zhang, N. Guo, F. Xu, Dr. X. Qian, Prof. Y. Zhao
School of Environmental Science and Engineering, Shanghai Jiao Tong University
800 Dongchuan Road, Shanghai 200240 (China)
E-mail: yixin.zhao@sjtu.edu.cn

Supporting information for this article can be found under: http://dx.doi.org/10.1002/anie.201606801.

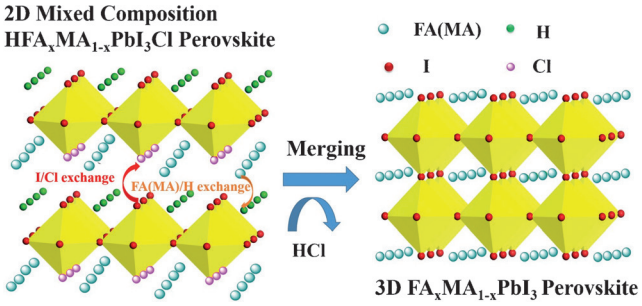

Scheme 1. Transformation of the 2D mixed composition A_2BX_4 of $HMA_{1-x}FA_xPbI_3Cl$ (A = H, MA, FA, B = Pb, X = I, Cl) into 3D $MA_{1-x}FA_xPbI_3$. Here the cations of H, FA and MA should be randomly distributed at A sites.

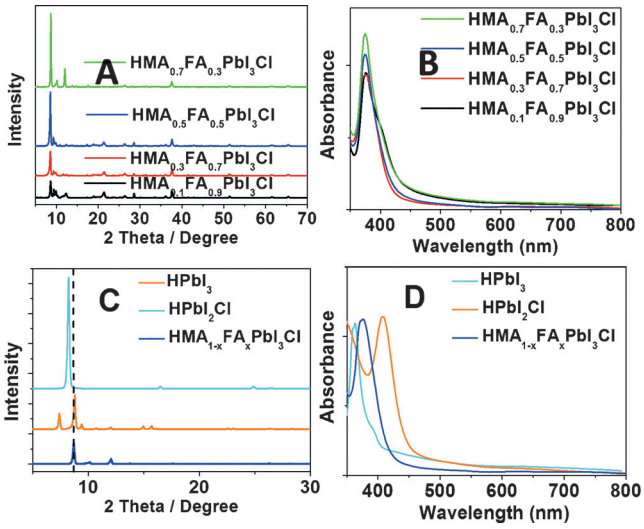

Figure 1. A) XRD and UV/Vis B) patterns of 2D $HMA_{1-x}FA_xPbI_3Cl$ ($x = 0.3$, 0.5, 0.7 and 0.9) precursor films; C) XRD patterns and D) UV/Vis spectrum of the $HMA_{0.7}FA_{0.3}PbI_3Cl$ precursor films as the typical 2D $HMA_{1-x}FA_xPbI_3Cl$ perovskite compared with the $HPbI_3$ and $HPbI_2Cl$ precursors films, respectively.

The cation A in classic 2D A_2BX_4 perovskite is usually long-chain alkyl ammonium to stabilize the 2D configuration by preventing the merging of the nearby 2D layers. In our designed easy-to-merge 2D $HMA_{1-x}FA_xPbI_3Cl$ perovskite, the H^+, MA^+, and FA^+ cations without long chains occupy the A site and the I and Cl with 3:1 ratio occupy the X site to form a 2D perovskite of A_2MX_4 (Scheme 1). Of course, the elemental ratio in the deposited film might be some different from the precursor solution owing to some uncerntainty during the spin-coating process. Although previously reported layer structure lead halide perovskites of $HPbI_3$ and $HPbI_2Cl$ with a similar unit frame are relatively stable,[22,37] this designed $HMA_{1-x}FA_xPbI_3Cl$ without long chain spacing is instable. Once the H/FA(MA) and Cl/I ion exchange reactions take place, the H^+ and Cl^- would form highly volatile HCl during the 2D–3D transformation and the HCl then releases into air. In contrast, the HCl/HI in previous reported assisted deposition of $MAPbI_3$ or $FAPbI_3$ is to modify the crystallization kinetics of perovskites.[15,25,37,38]

The deposited 2D $HMA_{1-x}FA_xPbI_3Cl$ perovskite films quickly turned to brown or dark even if they were kept in room temperature or under vacuum. Generally, the lower the FA content of x in the $HMA_{1-x}FA_xPbI_3Cl$, the quicker the precursor films turn to brown. Unfortunately, we cannot take the SEM or elemental characterization on these 2D perovskite precursor films because of their fast transformation into brown 3D perovskite films under vacuum. To obtain the reliable XRD and UV/Vis measurement, these deposited 2D perovskite films were immediately covered with PMMA and cooled down by an ice bag. The $HMA_{0.9}FA_{0.1}PbI_3Cl$ precursor films always turn brown during UV/Vis spectra and XRD measurement at room temperature even if they had been cooled by an ice bag. The XRD patterns of these ice-cooled stable $HMA_{1-x}FA_xPbI_3Cl$ ($x > 0.1$) precursor films are listed in the Figure 1 A. First of all, no typical pure $MAPbI_3$ or $FAPbI_3$ characteristic peaks of perovskites appear in the XRD patterns of these $HMA_{1-x}FA_xPbI_3Cl$ films. Although the MA:FA ratio are different in the $HMA_{1-x}FA_xPbI_3Cl$ precursor films, their XRD patterns have the same characteristic peaks at about 8.7°. Such sub-10 degree XRD peaks are similar to previous reported 2D lead halide perovskites or layer structure $HPbI_3$ and $HPbI_2Cl$ (Figure 1 C). The inorganic slab of $[PbX_6]$ can be oriented into ⟨100⟩, ⟨110⟩, and ⟨111⟩.[39] Here the interlayer space of about 1.0 nm derived from circa 8.7° peaks suggested that these peaks could be assigned as ⟨001⟩ peak because the circa 1 nm spacing distance is reasonable for the ⟨001⟩ layer thickness of 2D $HMA_{1-x}FA_xPbI_3Cl$ perovskite in consideration of circa 0.6 nm $[PbX_6]$ layer spacing and the circa 0.2 nm size of FA/MA cations on each side. Besides the similarity in their XRD pattern, these $HMA_{1-x}FA_xPbI_3Cl$ precursor films almost have UV/Vis spectra at the same wavelength with varied intensities. Both the XRD and UV/Vis results revealed that the $HMA_{1-x}FA_xPbI_3Cl$ might have very similar crystal structure as our designed 2D perovskite configuration. As illustrated in Scheme 1, the $[PbI_5Cl]$ frame unit of the 2D $HMA_{1-x}FA_xPbI_3Cl$ has the similar crystal structure with lattice parameters between the $[PbI_6]$ of $HPbI_3$ and $[PbI_4Cl_2]$ of $HPbI_2Cl$. Interestingly, both the characteristic XRD peaks and UV/Vis absorbance of the 2D $HMA_{1-x}FA_xPbI_3Cl$ perovskites located between those of $HPbI_3$ and $HPbI_2Cl$, which is reasonable based on their similarities in configuration and lattice parameter.

Since these 2D $HMA_{1-x}FA_xPbI_3Cl$ perovskites are instable and can turn to brown or black so quickly, we had to study their XRD and UV/Vis spectra under room temperature. Here we present the $HMA_{0.7}FA_{0.3}PbI_3Cl$ precursor of $MA_{0.7}FA_{0.3}PbI_3$ perovskite as the typical sample for investigation; other samples exhibited the similar crystal growth trend. Figure 2 A,B show the XRD pattern and UV/Vis spectra evolution of the deposited $HMA_{0.7}FA_{0.3}PbI_3Cl$ precursor film. First, both XRD and UV/Vis spectra show that the greenish–colorless precursor film can quickly grow into phase-pure $MA_{0.7}FA_{0.3}PbI_3$ perovskite with an absorbance onset edge at around 790 nm, which is consistent with the previously reported phase-pure $MA_{0.7}FA_{0.3}PbI_3$.[23] When the $HMA_{0.7}FA_{0.3}PbI_3Cl$ precursor film was annealed at 30 °C for 1 min, its characteristic XRD peaks decrease significantly

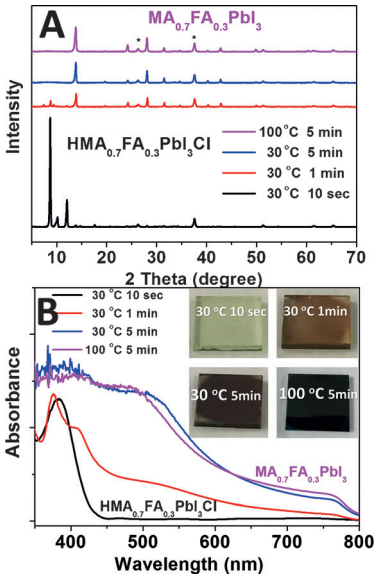

Figure 2. A) XRD and B) UV/Vis evolution of the transformation of $HMA_{0.7}FA_{0.3}PbI_3Cl$ into $MA_{0.7}FA_{0.3}PbI_3$ films annealed at 30 °C and 100 °C for different times.

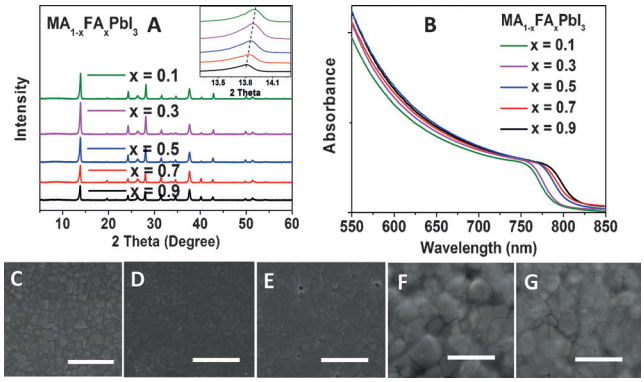

Figure 3. A) XRD patterns and B) UV/Vis spectrum of $MA_{1-x}FA_xPbI_3$ ($x = 0.1, 0.3, 0.5, 0.7, 0.9$) perovskite films prepared from $HMA_{1-x}FA_xPbI_3Cl$. SEM images of C) $MA_{0.9}FA_{0.1}PbI_3$, D) $MA_{0.7}FA_{0.3}PbI_3$, E) $MA_{0.5}FA_{0.5}PbI_3$, F) $MA_{0.3}FA_{0.7}PbI_3$ and G) $MA_{0.1}FA_{0.9}PbI_3$ films. The scale bar is 1 μm.

while characteristic XRD peaks of 3D $MA_{0.7}FA_{0.3}PbI_3$ perovskite appear. The UV/Vis spectra of $HMA_{0.7}FA_{0.3}PbI_3Cl$ precursor film annealed at 30 °C for 1 min also exhibited a $MA_{0.7}FA_{0.3}PbI_3$ related absorbance onset edge but with some remaining $HMA_{0.7}FA_{0.3}PbI_3Cl$ precursor films at short wavelength. After 30 °C annealing for 5 min, the $HMA_{0.7}FA_{0.3}PbI_3Cl$ precursor film completely transforms into phase pure $MA_{0.7}FA_{0.3}PbI_3$ perovskite based on its XRD and UV/Vis spectrum evolution. Although the $HMA_{0.7}FA_{0.3}PbI_3Cl$ perovskite can transform into phase-pure $MA_{0.7}FA_{0.3}PbI_3$ perovskite at room temperature, we still adopt the common 5 min 100 °C annealing to completely remove the solvent and other residues for deposition of $MA_{1-x}FA_xPbI_3$ ($x < 0.5$) using the $HMA_{1-x}FA_xPbI_3Cl$ samples. The high-temperature annealing can improve both the crystallinity and UV/Vis absorbance. For the crystallization process of the different $HMA_{1-x}FA_xPbI_3Cl$ perovskites, their transformation from $HMA_{1-x}FA_xPbI_3Cl$ into brown perovskite becomes slower with increasing x of FA content, which could be due to the steric effect of the FA cation to crystalize into 3D perovskite. For convenience, we adapted the 170 °C annealing to avoid the possible formation of δ-$FAPbI_3$ impurity during deposit of FA-rich perovskite of $MA_{1-x}FA_xPbI_3$ ($x > 0.5$) because the δ-$FAPbI_3$ phase is easy to form with the relatively low-temperature annealing process. We just use a simple and general annealing condition to demonstrate the facile deposition of high quality 3D $MA_{1-x}FA_xPbI_3$ by conversion of 2D $HMA_{1-x}FA_xPbI_3Cl$ precursor films. The adapted unspecific annealing treatments is not optimal for all the samples, which might account for the low PV efficiency for some $MA_{1-x}FA_xPbI_3$ perovskites solar cells.

Figure 3 A lists the XRD patterns of annealed $MA_{1-x}FA_xPbI_3$ ($x = 0.9, 0.7, 0.5, 0.3, 0.1$) perovskite films. First, no impurity peaks such as δ-$FAPbI_3$ were found in any of these samples. The 2D–3D transformation might account for the disappearance of yellow phase δ-$FAPbI_3$ formation. The 2D–3D conversion in our method only exhibits about 10% volume shrinkage as we measured on a profilometer. The strongest and characteristic XRD peaks of these $MA_{1-x}FA_xPbI_3$ ($x = 0.9$–0.1) perovskite films at about 14° all shifts with the FA content. The FA content-dependent XRD peak shift suggests the successful formation of phase-pure mixed-cation $MA_{1-x}FA_xPbI_3$ perovskites. The successful formation of phase-pure $MA_{1-x}FA_xPbI_3$ perovskites are also evidenced by the red-shift of the UV/Vis absorbance with an increase of FA content (Figure 3 B). In all, both XRD and UV/Vis results have confirmed the formation of phase-pure $MA_{1-x}FA_xPbI_3$. The SEM images of these $MA_{1-x}FA_xPbI_3$ perovskite films exhibit compact morphology (Figure 3 C–G); their AFM images and PL spectrum are given in the Supporting Information, Figures S1, S2. In contrast, the regular one-step method prepared $MA_{0.7}FA_{0.3}PbI_3$ exhibited the phase impurity of δ-$FAPbI_3$, coarse morphology, and low PV performance (Supporting Information, Figure S3). Furthermore, no detectable Cl signal could be found in the EDX analysis, revealing a complete removal of extra Cl in form of HCl from the 2D $HMA_{0.7}FA_{0.3}PbI_3Cl$ perovskite, as expected. The crystal-grain size of $MA_{1-x}FA_xPbI_3$ perovskites increases with the FA content, which could be attributed to the relatively slow crystallization process and the higher annealing temperature for these.

Here we fabricated planar-configuration perovskite solar cells devices using these $MA_{1-x}FA_xPbI_3$ perovskite planar films, which exhibited the typical J–V hysteresis for planar perovskite solar cells using c-TiO_2 as the electron-transfer layer (Supporting Information, Figure S4). First, these solar cells exhibited enhanced reproducibility in PV performance (Supporting Information, Table S1), suggesting the high reproducibility of our method. Figure 4 lists the typical J–V curves and IPCE of the $MA_{1-x}FA_xPbI_3$ solar cells. It is worth mentioning that the IPCE curves of these different $MA_{1-x}FA_xPbI_3$ solar cells match well with their UV/Vis spectra. The IPCE curves clearly demonstrate the successful formation of high-quality phase-pure $MA_{1-x}FA_xPbI_3$ perovskites with an extended light-absorbance range. The PV

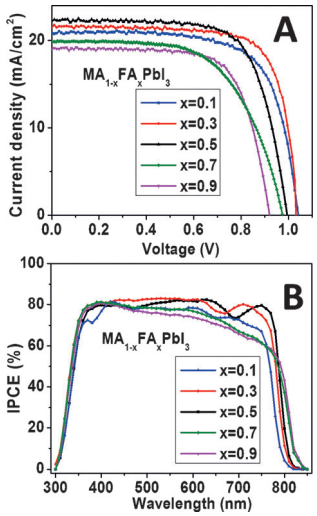

Figure 4. Typical *J*–*V* curves (A) and IPCE (B) of perovskite solar cells based on $MA_{1-x}FA_xPbI_3$ ($x = 0.1$, 0.3, 0.5, 0.7, 0.9) perovskite films.

performance of these $MA_{1-x}FA_xPbI_3$ perovskite solar cells are highly dependent on their composition of x. The J_{sc} of solar cells based on $MA_{0.7}FA_{0.3}PbI_3$ and $MA_{0.5}FA_{0.5}PbI_3$ is higher than the $MA_{0.9}FA_{0.1}PbI_3$. This can be attributed to the extended long wavelength absorbance as confirmed by IPCE curves (Figure 4B). Although the IPCE range of $MA_{0.3}FA_{0.7}PbI_3$ and $MA_{0.1}FA_{0.9}PbI_3$ has extended to even longer wavelength, their IPCE values are lower than the other perovskites. The previously reported high-quality $MA_{1-x}FA_xPbI_3$ by Han et al. also present the similar phenomenon that not all of the high-quality $MA_{1-x}FA_xPbI_3$ exhibited high PV performance.[23] This could due to the two facts: first, the $MA_{1-x}FA_xPbI_3$ ($x = 0.7$, 0.9) is not the optimal composition for the PV performance; second, the different composition $MA_{1-x}FA_xPbI_3$ perovskites require the specific optimal fabrication process. In general, the V_{oc} of these $MA_{1-x}FA_xPbI_3$ devices decreases with x of FA content, which could be due to the narrowing band gaps. As a compromise of J_{sc}, V_{oc}, and fill factor (FF), the $MA_{0.7}FA_{0.3}PbI_3$ solar cells exhibited the best efficiency. The champion $MA_{0.7}FA_{0.3}PbI_3$ based devices exhibited an efficiency of 17.02% with $V_{oc} = 1.03$ V, $J_{sc} = 22.03\ mA\,cm^{-2}$, and FF = 0.75 with 16.2% stable output (Supporting Information, Figure S5).

In summary, we successfully demonstrated a facile transformation of novel 2D $HMA_{1-x}FA_xPbI_3Cl$ ($x = 0.1$–0.9) perovskite into high-quality phase-pure 3D $MA_{1-x}FA_xPbI_3$ perovskite exhibiting the extended absorbance edge and IPCE range. The H and Cl used in the 2D perovskite with lower bond affinity than MA/FA and I in crystal structure was total removed during the 2D–3D conversion. In all, transformation of instable 2D mixed composition lead halide perovskite of $HMA_{1-x}FA_xPbI_3Cl$ into 3D high-quality phase-pure mixed-cation lead halide perovskite is an effective and facile method to deposit high-quality mixed-cation $MA_{1-x}FA_xPbI_3$ perovskite films. This 2D/3D transformation strategy would be a promising and potential candidate for one-step preparation of high-quality difficult-to-synthesize mixed-composition perovskites in the future.

Acknowledgements

Y.Z. acknowledges the support of the NSFC (Grant 51372151 and 21303103) and Huoyingdong Grant (151046).

Keywords: 2D perovskites · 2D–3D conversion · ion exchange · mixed-cation perovskites · perovskite solar cells

How to cite: *Angew. Chem. Int. Ed.* **2016**, *55*, 13460–13464
Angew. Chem. **2016**, *128*, 13658–13662

[1] A. Kojima, K. Teshima, Y. Shirai, T. Miyasaka, *J. Am. Chem. Soc.* **2009**, *131*, 6050–6051.
[2] J.-H. Im, C.-R. Lee, J.-W. Lee, S.-W. Park, N.-G. Park, *Nanoscale* **2011**, *3*, 4088–4093.
[3] N. J. Jeon, J. H. Noh, Y. C. Kim, W. S. Yang, S. Ryu, S. I. Seok, *Nat. Mater.* **2014**, *13*, 897–903.
[4] J. Burschka, N. Pellet, S. J. Moon, R. Humphry-Baker, P. Gao, M. K. Nazeeruddin, M. Gratzel, *Nature* **2013**, *499*, 316–319.
[5] M. M. Lee, J. Teuscher, T. Miyasaka, T. N. Murakami, H. J. Snaith, *Science* **2012**, *338*, 643–647.
[6] R. F. Service, *Science* **2014**, *344*, 458.
[7] H.-S. Kim, C.-R. Lee, J.-H. Im, K.-B. Lee, T. Moehl, A. Marchioro, S.-J. Moon, R. Humphry-Baker, J.-H. Yum, J. E. Moser, M. Gratzel, N.-G. Park, *Sci. Rep.* **2012**, *2*, 1–7.
[8] T. Zhang, Y. Zhao, *Acta Chim. Sinica* **2015**, *73*, 202–210.
[9] W. Chen, Y. Wu, Y. Yue, J. Liu, W. Zhang, X. Yang, H. Chen, E. Bi, I. Ashraful, M. Grätzel, L. Han, *Science* **2015**, *350*, 944–948.
[10] J. You, L. Meng, T.-B. Song, T.-F. Guo, Y. Yang, W.-H. Chang, Z. Hong, H. Chen, H. Zhou, Q. Chen, Y. Liu, N. De Marco, Y. Yang, *Nat. Nanotechnol.* **2015**, *11*, 75–81.
[11] A. Mei, X. Li, L. Liu, Z. Ku, T. Liu, Y. Rong, M. Xu, M. Hu, J. Chen, Y. Yang, M. Grätzel, H. Han, *Science* **2014**, *345*, 295–298.
[12] X. Li, M. Tschumi, H. Han, S. S. Babkair, R. A. Alzubaydi, A. A. Ansari, S. S. Habib, M. K. Nazeeruddin, S. M. Zakeeruddin, M. Grätzel, *Energy Technol.* **2015**, *3*, 551–555.
[13] X. Li, M. Ibrahim Dar, C. Yi, J. Luo, M. Tschumi, S. M. Zakeeruddin, M. K. Nazeeruddin, H. Han, M. Grätzel, *Nat. Chem.* **2015**, *7*, 703–711.
[14] W.-J. Yin, T. Shi, Y. Yan, *Adv. Mater.* **2014**, *26*, 4653–4658.
[15] Y. Zhao, K. Zhu, *Chem. Soc. Rev.* **2016**, *45*, 655–689.
[16] S. Wozny, M. Yang, A. M. Nardes, C. C. Mercado, S. Ferrere, M. O. Reese, W. Zhou, K. Zhu, *Chem. Mater.* **2015**, *27*, 4814–4820.
[17] D. P. McMeekin, G. Sadoughi, W. Rehman, G. E. Eperon, M. Saliba, M. T. Hörantner, A. Haghighirad, N. Sakai, L. Korte, B. Rech, M. B. Johnston, L. M. Herz, H. J. Snaith, *Science* **2016**, *351*, 151–155.
[18] N. Pellet, P. Gao, G. Gregori, T.-Y. Yang, M. K. Nazeeruddin, J. Maier, M. Grätzel, *Angew. Chem. Int. Ed.* **2014**, *53*, 3151–3157; *Angew. Chem.* **2014**, *126*, 3215–3221.
[19] N. J. Jeon, J. H. Noh, W. S. Yang, Y. C. Kim, S. Ryu, J. Seo, S. I. Seok, *Nature* **2015**, *517*, 476–480.
[20] W. S. Yang, J. H. Noh, N. J. Jeon, Y. C. Kim, S. Ryu, J. Seo, S. I. Seok, *Science* **2015**, *348*, 1234–1237.
[21] J.-W. Lee, D.-J. Seol, A.-N. Cho, N.-G. Park, *Adv. Mater.* **2014**, *26*, 4991–4998.
[22] F. Wang, H. Yu, H. H. Xu, N. Zhao, *Adv. Funct. Mater.* **2015**, *25*, 1120–1126.
[23] J. Liu, Y. Shirai, X. Yang, Y. Yue, W. Chen, Y. Wu, A. Islam, L. Han, *Adv. Mater.* **2015**, *27*, 4918–4923.
[24] M. R. Filip, G. E. Eperon, H. J. Snaith, F. Giustino, *Nat. Commun.* **2014**, *5*, 5757.
[25] Y. Zhao, K. Zhu, *J. Phys. Chem. Lett.* **2014**, *5*, 4175–4186.

[26] B.-J. Kim, D. H. Kim, Y.-Y. Lee, H.-W. Shin, G. S. Han, J. S. Hong, K. Mahmood, T. Ahn, Y.-C. Joo, K. S. Hong, N.-G. Park, S. Lee, H. S. Jung, *Energy Environ. Sci.* **2014**, *8*, 916 – 921.
[27] W. Ke, G. Fang, J. Wan, H. Tao, Q. Liu, L. Xiong, P. Qin, J. Wang, H. Lei, G. Yang, M. Qin, X. Zhao, Y. Yan, *Nat. Commun.* **2015**, *6*, 6700.
[28] L. K. Ono, S. Wang, Y. Kato, S. R. Raga, Y. Qi, *Energy Environ. Sci.* **2014**, *7*, 3989 – 3993.
[29] M. Liu, M. B. Johnston, H. J. Snaith, *Nature* **2013**, *501*, 395 – 398.
[30] Y. Zhou, M. Yang, A. L. Vasiliev, H. F. Garces, Y. Zhao, D. Wang, S. Pang, K. Zhu, N. P. Padture, *J. Mater. Chem. A* **2015**, *3*, 9249 – 9256.
[31] Y. Zhou, O. S. Game, S. Pang, N. P. Padture, *J. Phys. Chem. Lett.* **2015**, *6*, 4827 – 4839.
[32] T. Zhang, N. Guo, G. Li, X. Qian, Y. Zhao, *Nano Energy* **2016**, *26*, 50 – 56.
[33] M. Era, S. Morimoto, T. Tsutsui, S. Saito, *Appl. Phys. Lett.* **1994**, *65*, 676 – 678.
[34] D. B. Mitzi, S. Wang, C. A. Feild, C. A. Chess, A. M. Guloy, *Science* **1995**, *267*, 1473 – 1476.
[35] L. Dou, A. B. Wong, Y. Yu, M. Lai, N. Kornienko, S. W. Eaton, A. Fu, C. G. Bischak, J. Ma, T. Ding, N. S. Ginsberg, L.-W. Wang, A. P. Alivisatos, P. Yang, *Science* **2015**, *349*, 1518 – 1521.
[36] S. Colella, E. Mosconi, P. Fedeli, A. Listorti, F. Gazza, F. Orlandi, P. Ferro, T. Besagni, A. Rizzo, G. Calestani, G. Gigli, F. De Angelis, R. Mosca, *Chem. Mater.* **2013**, *25*, 4613 – 4618.
[37] G. Li, T. Zhang, Y. Zhao, *J. Mater. Chem. A* **2015**, *3*, 19674 – 19678.
[38] G. E. Eperon, S. D. Stranks, C. Menelaou, M. B. Johnston, L. M. Herz, H. J. Snaith, *Energy Environ. Sci.* **2014**, *7*, 982 – 988.
[39] D. B. Mitzi, *J. Mater. Chem.* **2004**, *14*, 2355 – 2365.

Received: July 13, 2016
Revised: August 12, 2016
Published online: September 26, 2016

